NOTES AND CORRESPONDENCE

Entrainment and Transport in Idealized Three-Dimensional Gravity Current Simulation

YU-HENG TSENG*

Computational Research Division, Lawrence Berkeley National Laboratory, Berkeley, California

DAVID E. DIETRICH

AcuSea, Inc., Albuquerque, New Mexico

(Manuscript received 4 March 2005, in final form 2 March 2006)

ABSTRACT

A purely z-coordinate Dietrich/Center for Air Sea Technology (DieCAST) ocean model is applied to the Dynamics of Overflow Mixing and Entrainment (DOME) idealized bottom density current problem that is patterned after the Denmark Strait. The numerical results show that the background viscosity plays a more important role than the chosen coordinate system in the entrainment and mixing if the background viscosity is not small enough. Both higher horizontal viscosity and coarser resolution leads to slower along-slope propagation. Reducing vertical mixing parameterization also leads to slower along-slope propagation with thicker plume size vertically. The simulation gives consistent results for the moderate- and fine-resolution runs. At a very coarse grid the dense water descends more slowly and is mainly dominated by diffusion. Time-averaged downstream transport and entrainment are not very sensitive to viscosity after the flow reaches its quasi-steady status. However, more realistic eddies and flow structures are found in low-viscosity runs. The results show good convergence of the resolved flow as expected and clarify the effects of numerical dissipation/mixing on overflow modeling. Larger numerical dissipation is not required nor recommended in z-coordinate models.

1. Introduction

Modeling dense bottom density currents emanating from sill overflows is of major research interest (e.g., Peters et al. 2005; Killworth 2001; Killworth and Edwards 1999). The Dynamics of Overflow Mixing and Entrainment (DOME) experiments established an idealized model setup to investigate the dynamics of bottom plumes. The configuration is mainly patterned after the sill overflow from the Denmark Strait between Greenland and Iceland. The importance of meandering and eddies for mixing overflow plumes has been noted by previous studies (Jiang and Garwood 1996; Girton and Sanford 2003; Cenedese et al. 2004). DOME configuration is highly idealized and primarily intended to test a model's ability. Ezer and Mellor (2004) apply a new hybrid ocean model, derived from the original σ-coordinate Princeton Ocean Model (SPOM), to simulate dense water overflow experiment in the DOME configuration. They also compared their SPOM results with z-coordinate POM (ZPOM). Legg et al. (2006) simulated the same configuration using z-coordinate Massachusetts Institute of Technology (MIT) general circulation model (MITgcm) and Hallberg Isopycnal Model (HIM). These studies provided a benchmark comparison for different models, and all models simulated some observed characteristics of the Denmark Strait plume (Girton and Sanford 2003) quite well, except ZPOM. Ezer and Mellor (2004) inferred that the problems in ZPOM were inherent to stair-step representation of the ocean bathymetry, including the need for large viscosity to maintain numerical stability. However, using another z-coordinate model, our re-

* Current affiliation: Department of Atmospheric Sciences, National Taiwan University, Taipei, Taiwan.

Corresponding author address: Yu-Heng Tseng, Department of Atmospheric Sciences, National Taiwan University, No. 1, Roosevelt Road, section 4, Taipei, Taiwan 10673.
E-mail: yhtseng@webmail.as.ntu.edu.tw

sults suggest that viscosity effects may play more important roles than the chosen coordinate in a model. The use of stair-step topography in z-coordinate models does not necessitate the use of large viscosity. In fact, using large viscosity misrepresents ocean physics and fluid dynamic behaviors. Further, theoretical analysis shows that it is much easier to demonstrate convergence in z-coordinate models than in other models as illustrated in this paper. The competing effects of horizontal and vertical background viscosity are clearly presented. ZPOM's nonrobustness problem may be overcome by using a quadratic-conserving second-order advection approximation (Lilly 1965), even when viscosity is very small. The large underlying dissipation and diffusion may result from the model numerics. Thus, the inference that all z-coordinate models have severe robustness and accuracy problems similar to ZPOM seems mistaken.

Ezer and Mellor (2004) suggest that coarse-resolution z-coordinate models need larger horizontal diffusivity than do terrain-following models in order to maintain numerical stability. They further found that increasing horizontal diffusion caused a thinner bottom boundary layer (BBL) and a bottom density current that extended further downslope in SPOM, but caused a thicker BBL and limited downslope density current extension in ZPOM. Contrary to their interpretation that z-coordinate models require large explicit viscosity, Dietrich et al. (2004, hereinafter D04), showed that lower background viscosity is required to maintain density currents sufficiently robust to give realistic Gulf Stream separation, mean path, and dynamics including flattening of the interior isopycnals between the separated Gulf Stream and New England shelf break. In particular, D04 used small explicit viscosity/diffusivity ($20\ m^2\ s^{-1}$) and investigated viscosity effects on model results. The poor results in ZPOM model may result from its numerics, not its coordinate.

D04 used a purely z-coordinate model. It did not include the thin-shell BBL approach (e.g., Dietrich et al. 1987; Ezer 1990; Beckmann and Doscher 1997; Killworth and Edwards 1999; Song and Chao 2000), partial cells (Adcroft et al. 1997; Pacanowski and Gnanadesikan 1998), or immersed boundary method (IBM) (Tseng and Ferziger 2003, 2004; Tseng et al. 2005). The bottom density current in North Atlantic Ocean was not resolved by the climatological data used for initial conditions and thus developed spontaneously in D04. Thus, although not resolving the BBL, the modeled bottom density current was sufficiently robust to affect Gulf Stream separation and ensuing dynamics.

The objectives of this paper are to study the entrainment and mixing in DOME configuration using a purely z-coordinate model with a high-order, conservative scheme, and to investigate the effects of viscosity/diffusivity on the density current flows. We further clarify that numerical instability relates closer to the robustness of the model rather than the chosen coordinate. The horizontal and vertical viscosity shows competing influence on the model results. The convergence of model results as resolution increases demonstrates the required resolution (necessary condition) for any z-coordinate model and provides a guideline for further model comparisons within DOME experiments. The effects of viscosity and resolution are as expected. The mesoscale (low frequency) energy spectrum is not sensitive to either viscosity or resolution. However, the small-scale (high frequency) energy spectrum depends on resolution and is not sensitive to viscosity when it is small enough. As in D04, we also find that large viscosity or extremely high resolution is not required to realistically simulate density current plume in a purely z-coordinate model. Less robust or low-order numerical approximation needs higher resolution to obtain the same accuracy level (Ferziger and Perić 2002). Nondissipative, higher-order, and robust numerical algorithms should be used to achieve the highest accuracy and stability on a reasonable grid no matter what vertical coordinate is used.

Note that Penduff et al. (2002) suggested that smoothing the topography in a z-coordinate model results in simulations that qualitatively resemble those from a σ-coordinate model. This is based on the fact that σ-coordinate models use a smooth function to approximate or filter the irregular bathymetry. However, real bathymetry is not smooth and cannot be approximated more accurately (less than one grid point) unless more information from bathymetry is used (e.g., Adcroft et al. 1997; Tseng and Ferziger 2003). Filtering the bathymetry deteriorates accuracy and thus is not recommended because bathymetry details strongly affect ocean flows in reality.

The model formulation is provided in section 2. Section 3 reports the numerical results and shows that purely z-coordinate models can give robust and accurate overflow results using practical resolution. Entrainment and mixing are quantified in terms of resolution and viscosity effects. These effects are clearly shown in the energy spectrum. We clearly illustrate that the robustness of solution is determined by its numerical procedure. Accuracy depends significantly on the order of the numerics as well as the chosen coordinate and should be carefully examined (Sanderson 1998). The adequateness of z-coordinate models for DOME configuration is discussed in section 4. Finally, conclusions are provided in section 5.

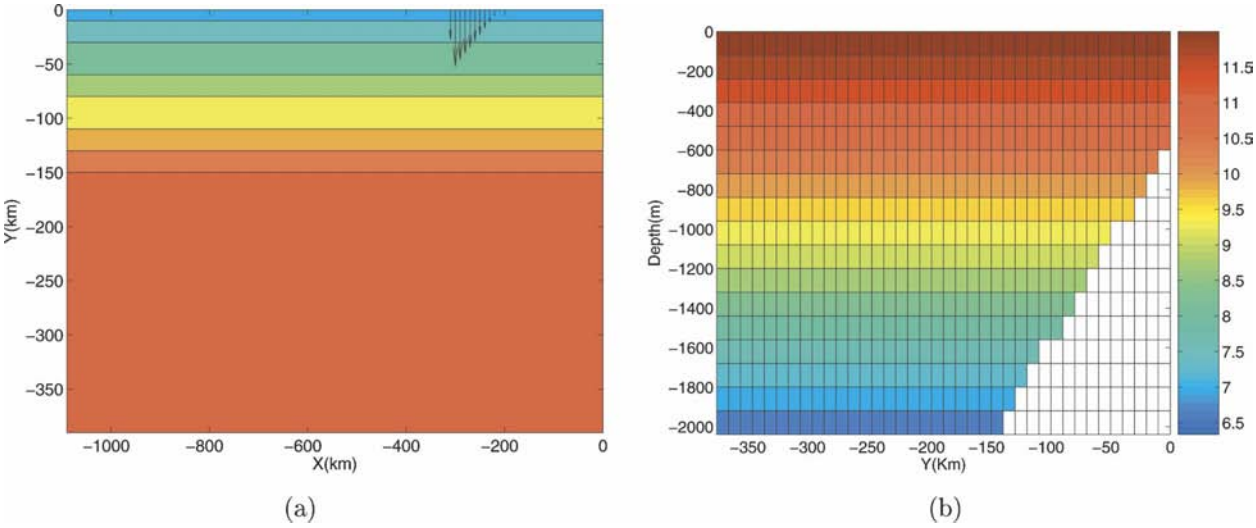

FIG. 1. (a) The horizontal domain and northern inflow velocity vector at the bottom (top of panel) on a 10-km-resolution grid. The color scale represents the bathymetry depth contours. (b) Illustration of latitudinal–vertical grid and initial temperature stratification on a 10-km-resolution grid.

2. Model formulation

To demonstrate the ability of z-coordinate models to model bottom density currents, we use a purely z-coordinate version of the DieCAST model (Dietrich 1997) in this study, as did D04. The DieCAST model evolved from the Sandia Ocean Modeling System (SOMS) model, which used a thin-shell BBL approach (Dietrich et al. 1987). The latest version of DieCAST used the IBM approach to better represent the bathymetry (Tseng and Ferziger 2003; Tseng et al. 2005). The IBM specifies a body force along the boundary in such a way as to simulate the presence of bottom topography accurately instead of stair-step approximation in a z-level model (Tseng and Ferziger 2003). The main advantage of IBM is its simplicity and accurate representation of boundary (either coastal or bottom boundary). However, none of these approaches is used here because our objective is to show that, given a realistic bottom stress (e.g., from a thin-shell BBL model), a higher-order z-coordinate model with lower numerical dissipation can adequately model bottom density currents using moderate resolution.

We thus apply the purely z-coordinate DieCAST model to the idealized density current problem in DOME configuration, patterned after the observed density current spilling over the Denmark Strait sill. The DieCAST model uses a mixed Arakawa A and C grid, fourth-order central difference, conservative numerical scheme (Dietrich et al. 2004). The idealized DOME overflow configuration has been outlined in Ezer and Mellor (2004) and Legg et al. (2006). An 1100 km (longitude) by 400 km (latitude) region is modeled (Fig. 1). The northernmost latitude is 600 m deep. A 1% shelf slope brings it to maximum depth 2160 m at 156 km offshore (Fig. 1b). The depth is uniformly 2160 m farther south. This domain is the same as the high-resolution experiment Z4 in Ezer and Mellor (2004). A list of dimensional parameters for the overflow configuration is provided in Table 1 and compared with those in Legg et al. (2006). Bottom stress is parameterized with a quadratic drag law with $C_d = 0.002$. The model is documented in detail in a user's manual (Tseng and Dietrich 2005), including the downloadable adaptation used for the results shown herein.

Within the basic DOME configuration, we have carried out simulations for 11 combinations of resolution and viscosity (Table 2). The vertical and horizontal resolution in the coarsest grid (RCL) is 120 m and 50 km uniformly. RCL, R0L, R1L, R2L, and R3L runs illustrate resolution sensitivity using low horizontal viscosity (υ_h)/diffusivity (κ_h) (υ_h, $\kappa_h = 4\ \mathrm{m^2\ s^{-1}}$). The vertical mixing is parameterized using a modified Richardson-number-based vertical viscosity and diffusivity with background values of $1 \times 10^{-6}\ \mathrm{m^2\ s^{-1}}$ (Pacanowski and Philander 1981). These conditions give typical cell Reynolds number $O(100)$. We have tested even lower viscosity/diffusivity (υ_h, $\kappa_h = 1\ \mathrm{m^2\ s^{-1}}$) and no significant difference is found; results are almost independent of viscosity/diffusivity as we further reduce the values. The R2L run converges well to R3L run except more small-scale eddies occur in R3L. An additional simulation with a second-order, central difference advection scheme is also performed for the comparison (R2L2O).

TABLE 1. Dimensional parameters for the three-dimensional overflow configuration.

Dimensional parameter	Legg et al. (2006)	Current study
Domain length L_x (km)	1000–2000	1100
Domain width L_y (km)	600	400
Inflow depth H_i (m)	600	600
Maximum depth L_z (m)	3600	2200
Drag coefficient C_d	2×10^{-3}	2×10^{-3}

The advection scheme has dominant influence on the accuracy. Note that the fourth-order numerics can give little overshooting with very low viscosity. The cell Reynolds (Peclet) number can be significantly relaxed [O(10–1000)] using higher-order numerics. Overshoots (oscillations) can be fully eliminated by a coordinate invariant streamwise upwind formulation for advection while maintaining high-order accuracy (Ferziger and Tseng 2004), but the method is not adopted here. Using the dissipative (upwind-biased–monotonic) scheme for advection is not recommended to study turbulent mixing and entrainment because the numerical diffusion resulting from the high-order, upwind-biased (monotonic) schemes is hardly controlled and contributes significantly to the mixing events (Gresho and Lee 1981). The artificial diffusion effects resulting from numerical schemes are beyond the scope of this paper.

The effects of viscosity are further investigated using a multiprogram-component hand-shaking (MPH) library (He and Ding 2005). The MPH library is particularly useful to assess the influence of several parameters simultaneously on a parallel platform. The documentation and source codes can be downloaded from the Web (http://hpcrd.lbl.gov/SCG/acpi/MPH). Cases 4–6 present the effects of horizontal viscosity/diffusivity (Table 2). The highest horizontal viscosity/diffusivity ($\nu_h/k_h = 200/100\ \mathrm{m^2\ s^{-1}}$) in R2HDI shows viscosity sensitivity. It is well known that increasing viscosity also increases the numerical dissipation similar to the effects of an upwind-biased advection scheme. An accurate simulation requires appropriate background viscosity. The effects of vertical background viscosity are presented in cases 7–8. We also include an additional case without vertical mixing scheme to investigate the influence of vertical parameterization (R2LNP).

The northern inflow is bottom concentrated and geostrophically balanced. Inflow is imposed at the northern boundary ($x = -200$ km to $x = -300$ km), patterned after the Denmark Strait (Fig. 1a). The bottom (top) layer inflow temperature increases linearly from 5.3°C (13°C) on its west side to 9.9°C (15°C) on its east side. The inflow is stably stratified and bottom-concentrated (at 600 m), with a total of 4.98 Sv ($1\ \mathrm{Sv} \equiv 10^6\ \mathrm{m^3\ s^{-1}}$) inflow. Initial conditions are identical to the DOME conditions used by Ezer (2005) and Legg et al. (2006). The eastern and southern boundaries are closed. The western boundary is open, using an upwind-based, convective-type outflow condition. The convective open boundary condition is adequate since the signal propagates strictly downstream for internal Kelvin waves and advection. The normal velocity at the open boundary is adjusted to give no net inflow into the modeled region. Free-slip and no-flux boundary conditions are applied at closed boundaries. The bottom boundary uses a no-slip condition parameterized by nonlinear drag. To analyze the development of the dense water plume, we also inject a tracer between depth 300 and 600 m in the inflow. Initially the tracer concentration is zero everywhere.

3. Results

a. General description

Figure 2 shows snapshots of bottom boundary tracer concentration (c) on four different model days from the 2.5-km resolution run (R3L). We include results up to 20 days to illustrate the initial development of the

TABLE 2. Comparison of dimensional parameters in different runs for the three-dimensional overflow.

Dimensional parameter	Horizontal viscosity/diffusivity ν_h/κ_h ($\mathrm{m^2\ s^{-1}}$)	Vertical background viscosity ν_v ($10^{-4}\ \mathrm{m^2\ s^{-1}}$)	Horizontal resolution Δx (km)	Vertical resolution Δz (m)
Case 1 (RCL)	4/4	0.1	50	120
Case 2 (ROL)	4/4	0.1	20	120
Case 3 (R1L)	4/4	0.1	10	120
Case 4 (R2L)	4/4	0.1	5	60
Case 5 (R2MDI)	20/20	0.1	5	60
Case 6 (R2HDI)	200/100	0.1	5	60
Case 7 (R2LHP)	4/4	80	5	60
Case 8 (R2LMP)	4/4	2	5	60
Case 9 (R2LNP)	4/4	—	5	60
Case 10 (R2L2O)	4/4	0.1	5	60
Case 11 (R3L)	4/4	0.1	2.5	30

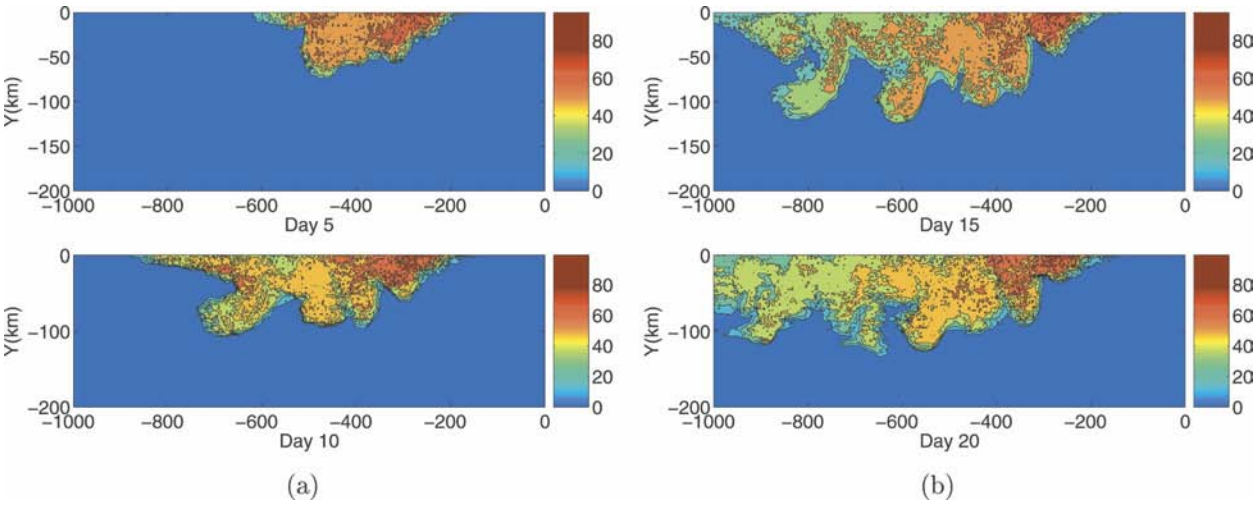

FIG. 2. Instantaneous bottom boundary tracer concentration (just above the topography) in the R3L run on four different days: (a) days 5 and 10; (b) days 15 and 20. The concentration is identified by percentage (%). Contours are plotted every 10%. Inflow is imposed between −200 and −300 km.

plume. That is about the time it takes for the inflow plume to reach the downstream outflow, and after this time the flow appears to approach a statistically quasi steady state. The longitudinal distance (alongshore) is shown up to 1000 km downstream. A quasi steady state is achieved after 25 days in our simulation in terms of plume thickness, width, and entrainment properties. The westward and downslope propagation of the dense bottom plume is clearly seen and similar to the observations reported in Girton and Sanford (2003). Earth rotation and the resultant topographic β effect have a major influence on downslope density current penetration and the growth of a large-amplitude wavelike structure, as expected from the geostrophic adjustment on the slope (Jiang and Garwood 1996; Cenedese et al. 2004). On a longer time scale, bottom-drag-induced secondary flow affects downslope penetration and entrainment. Most tracer dilution occurs around 50 km away from the coast ($y = -50$ km). Farther to the west ($x < -400$ km) there is stirring generated by large-amplitude filaments, but this does not appear to modify tracer concentration significantly. The instantaneous snapshots also demonstrate the small-scale structures responsible for mixing. Such small-scale structures are consistent with the property of high-order, nondissipative numerical schemes (Mittal and Moin 1997).

In general, many qualitative features in the current study resemble those presented in previous higher-resolution models (Ezer 2005; Legg et al. 2006). In particular, the deep water intrusion near $x = -500$ km is quite similar to nonhydrostatic, 0.5-km-resolution studies (Legg et al. 2006). Note that the current results show more eddy activity than previous z-coordinate models at the same resolution. Observations of overflows also indicate considerable variability and eddy activity (Girton and Sanford 2003). The results are different from those reported in ZPOM (Ezer and Mellor 2004), which show strongly diffused bottom plume and weak eddies. Ezer and Mellor (2004) argued that the ZPOM with either a 10- or 2.5-km grid shows more diapycnal mixing due to the large vertical mixing over the step topography than the σ-coordinate model does. It is evident that the frontal instability is resolved in the current simulation but not in ZPOM. We attribute this difference to the numerics (low numerical dissipation and high degree of numerical accuracy in DieCAST) rather than the coordinate. More discussion regarding to the resolution and viscosity is presented in the next section.

b. Sensitivity to resolution and viscosity

A resolution study is performed to analyze the accuracy of the current results ranging from 50 to 2.5 km. Figures 3 and 4 show one-day-averaged tracer concentration for all runs on model day 20 at the bottom boundary just above the topography (bottom-most cell) and at the sill level depth 600 m. In the medium-resolution (R2L, R2L2O) runs (Fig. 3), the plume distribution along the bottom bathymetry is quite similar to the higher-resolution runs except for some fine features along the front. The average size, structure, and thickness of the plume are even closer in R2L and R3L runs. In the R2L2O run, a second-order advection scheme produces larger dispersion errors that introduce larger oscillations; however, the general structure is still very close to the R2L run. The 2.5-km resolution run (R3L) includes more fine- and small-scale structures

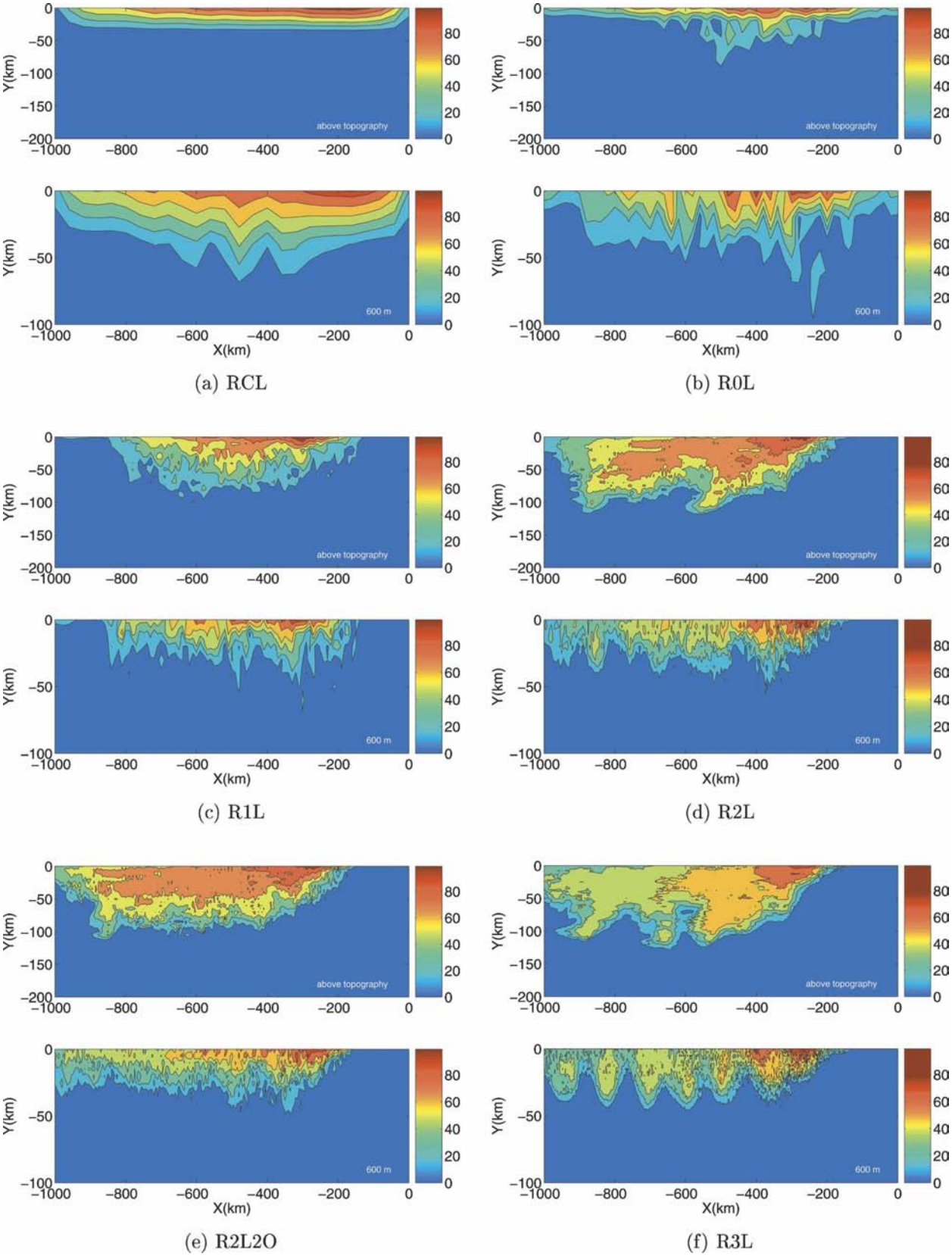

FIG. 3. One-day-averaged tracer concentration at (top) bottom boundary and (bottom) sill level depth 600 m on model day 20. The bottom boundary is the boundary cell just above the topography. The concentration is identified by percentage (%). Contours are plotted every 10%. Inflow is imposed between −200 and −300 km: Runs (a) RCL, (b) R0L, (c) R1L, (d) R2L, (e) R2L2O, and (f) R3L.

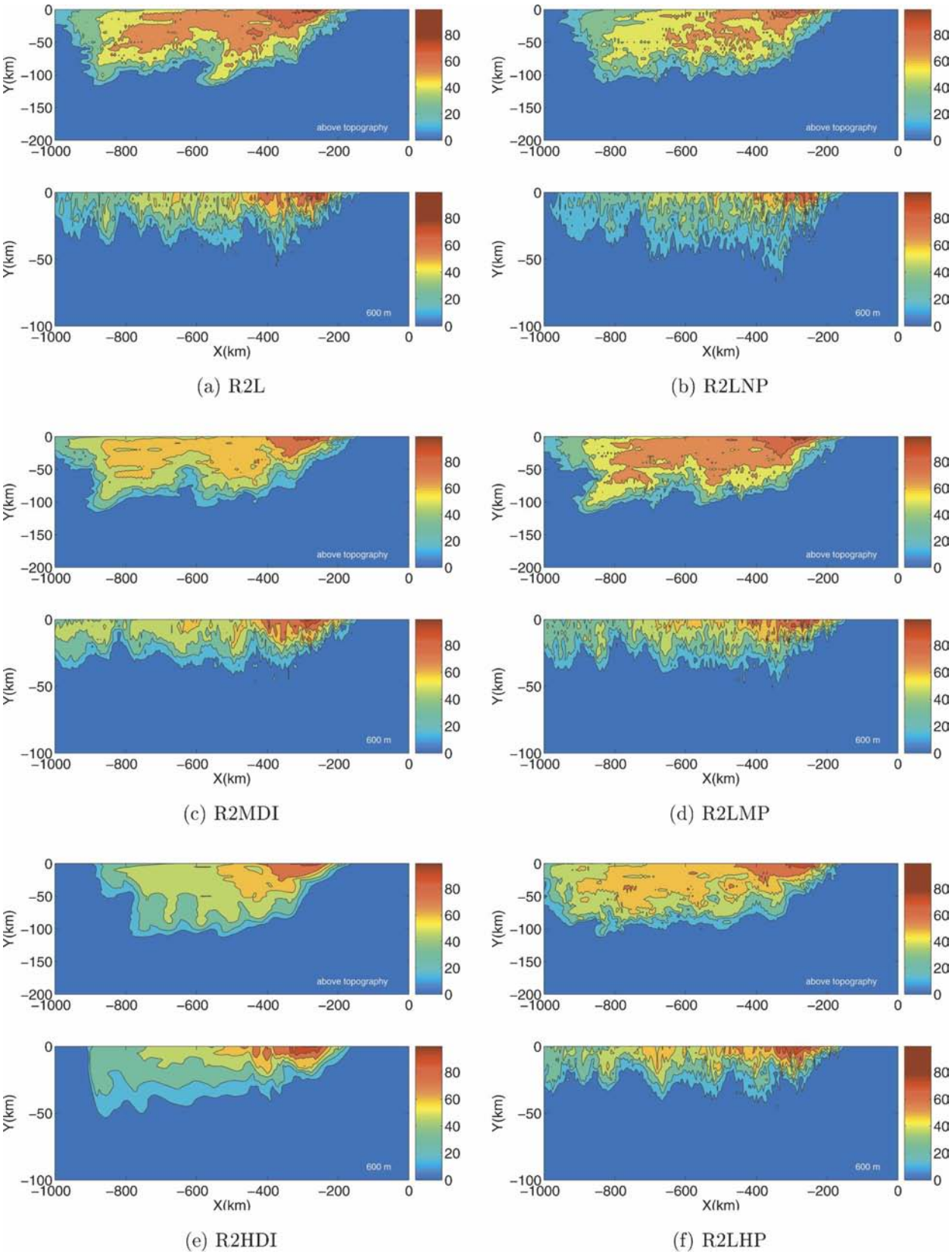

FIG. 4. As in Fig. 3 but for runs (a) R2L, (b) R2LNP, (c) R2MD1, (d) R2LMP, (e) R2HD1, and (f) R2LHP.

than the 5-km resolution case (R2L). All of the comparisons were run with low horizontal viscosity ($\nu_h = 4$ $m^2 s^{-1}$).

These results clearly illustrate the growth of the plume and its westward propagation. The westward and downslope propagation of the dense bottom plume involves not only bottom Ekman flows, but also the mixing due to eddies. It is interesting to see the growth and downstream propagation of the large-amplitude wavelike structures observed at the sill level in the medium- (R2L) and highest- (R3L) resolution runs. These structures are commonly seen along the coast and are possibly due to baroclinic instability (Tseng and Ferziger 2001). The wavelike structures in R2L run are comparable in size to those in the highest-resolution run (R3L) and have size of roughly 50 km. The Rossby radius of deformation (R_0) here is about 45 km, so that the structures are marginally resolved with a 10-km horizontal resolution (R1L) but fully resolved with a 5 km or higher resolution. It is clear that both R0L and RCL runs cannot resolve the horizontal scale of R_0. Besides resolving the Rossby radius of deformation, theoretical analysis shows that, in order to resolve the overflow down the slope, both vertical and horizontal resolutions need to satisfy the following criteria (Winton et al. 1998):

$$\Delta X < h/\tan(\alpha) \quad \text{and} \quad \Delta Z < h, \tag{1}$$

where h is the thickness of the overflow and α is the topographic slope; $\tan(\alpha)$ is 0.01 in our study. If the thickness of overflow is taken as the observed thickness (160 m) below the Denmark Strait (Girton and Sanford 2003), ΔX has to be smaller than 16 km and ΔZ has to be smaller than 160 m. However, in order to resolve the sharp change, we need at least two or three points across the overflow; that is, actual grid size Δx (Δz) has to be smaller than $\Delta X/2$ ($\Delta Z/2$). This is consistent with our finding that 10-km resolution can only partially resolve the overflow while 5- or 2.5-km resolution can fully resolve the overflow plumes. The turbulent mixing occurring within the grid size is then limited by the grid size and has to be represented by turbulent mixing parameterization. The results clarify that a model resolution of 5 km is sufficient to resolve important meanders and structures for mixing of overflow plumes. Among the cases in which the overflow can be partially or fully resolved, slower longitudinal (along-slope) propagation is also observed in the coarser-resolution run.

Note that the vertical resolution is uniformly 60 and 30 m in R2L and R3L runs, respectively. Neither the IBM or partial-cell approach is used to better represent the slope. The current comparison represents the most general cases in z-coordinate models. Even though 5-km resolution is enough (sufficient) to resolve the 1% bottom slope from the analysis, the ability to fully resolve the topographical change depends significantly on the model's numerics rather than its coordinate. The grid resolution study illustrates the minimal requirement to fully resolve the overflow along the slope using z-coordinate models. For sigma and isopycnal coordinate models, the requirement is relaxed but is not easy to analyze because of the grid stretching close to the bathymetry and the coordinate transformation.

Figure 4 compares the effects of viscosity/diffusivity at 5-km resolution. The influence of horizontal viscosity/diffusivity is presented in the left column while the effect of vertical viscosity/diffusivity is shown in the right column. The eddies are strong and the plume front is sharp enough to support frontal instabilities in low-viscosity runs (R2L, R2LNP, and R2LMP). The difference between R2L and R2MDI runs is small. Even lower horizontal viscosity is applied and no significant difference is found. These results imply the asymptotic behavior of viscosity effects, which are independent of background viscosity if it is small enough. Figure 4e shows the highest horizontal viscosity run (R2HDI). It is evident that weaker eddies and smoother flow result in the highest dissipation simulation. Using large background viscosity damps finescale features that are ubiquitous in the low-viscosity runs. These small-scale features in low-viscosity runs are significantly nongeostrophic and have less vortex stretching constraint than larger scales. There are almost no eddies in the R2HDI run and the diffused front in this run causes a slower longitudinal propagation of the plume. Vertical mixing parameterization is removed in the R2LNP run. In the R2LHP run, the imposed vertical background viscosity is compatible with the eddy viscosity resulting from the vertical mixing parameterization. The comparison in the right panel shows slightly slower longitudinal propagation in the run without vertical parameterization, and this is mainly due to larger vertical thickening, discussed in later sections.

The current results clearly illustrate that z-coordinate models can transport dense fluid down the slope without excessive entrainment/mixing. Note that faster longitudinal propagation is also observed in the low horizontal viscosity run (R2L); however, the total transport is quite similar. The physical entrainment and transport will be quantified further in section 3d.

c. Energy spectrum

Examination of the power spectra of velocity fluctuations obtained using nondissipative, conservative schemes showed that the small turbulent scales are often more energetic than those in the upwind-biased

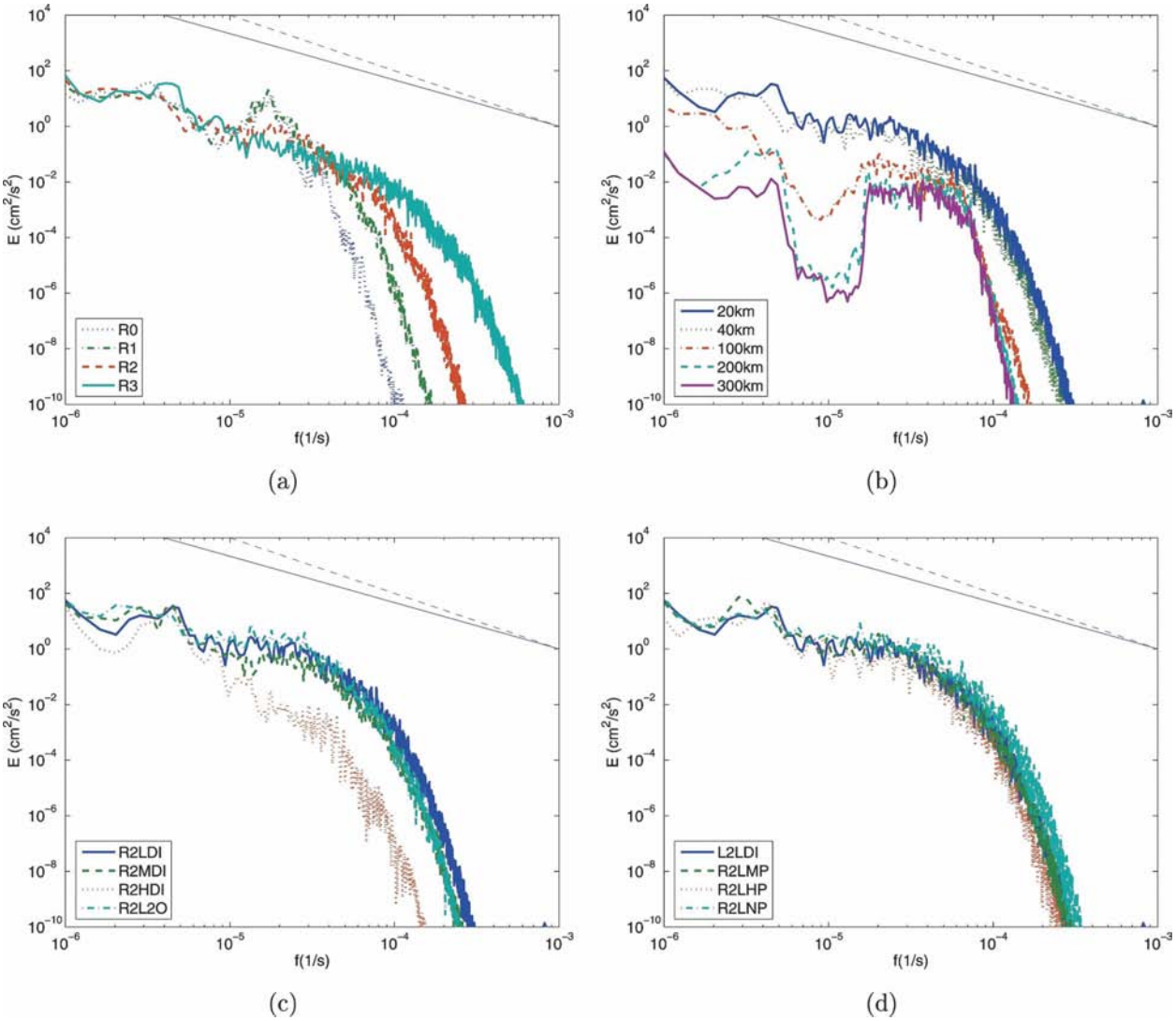

FIG. 5. (a) Comparison of energy spectrum at 40 km offshore for different resolution runs. (b) Energy spectrum vs offshore distance in case R2L. (c), (d) Illustration of the effects of explicit viscosity for different runs.

simulations and in better agreement with experiments over a wider range of wavenumbers (see, e.g., Kravchenko and Moin 2000; Mittal and Moin 1997). The viscosity sensitivity in the previous section confirms that smaller background viscosity in a nondissipative model produces more energy in the eddy fields. Figure 5a compares the energy spectrum at 40 km offshore for different resolution runs. More high-frequency energy and finer scales can be resolved with increasing resolution as expected. Lower-frequency energy spectrum represents the energy associated with large mesoscale motion and is similar in the comparison from R0 to R3. The solid line shown has slope 5/3 and the dashed line shown has slope 2. The slope of energy in the low-frequency range seems to have slope between 5/3 and 2.

Figure 5b compares the energy spectrum at depth 600 m as a function of offshore distance. Near the coast, the broad spectrum range suggests the nearshore bottom boundary flow is dominated by several instability mechanisms that have very broad scales. Note that the well-known "spectral gap" is evident when the sampling moves further offshore (Van der Hoven 1957; Pouquet et al. 1983; Dietrich 1977). The two spectral peaks represent two dominating types of flow: the quasi-horizontal mesoscale motions (time scales greater than a day) and small-scale motions. The large-scale feature is dominated by the mesoscale feature of density currents discussed in the previous section. The spectrum gap is associated with the Coriolis force offshore. The small-scale motion is dominated by ageostrophic flows. Additional tests show that, while reduc-

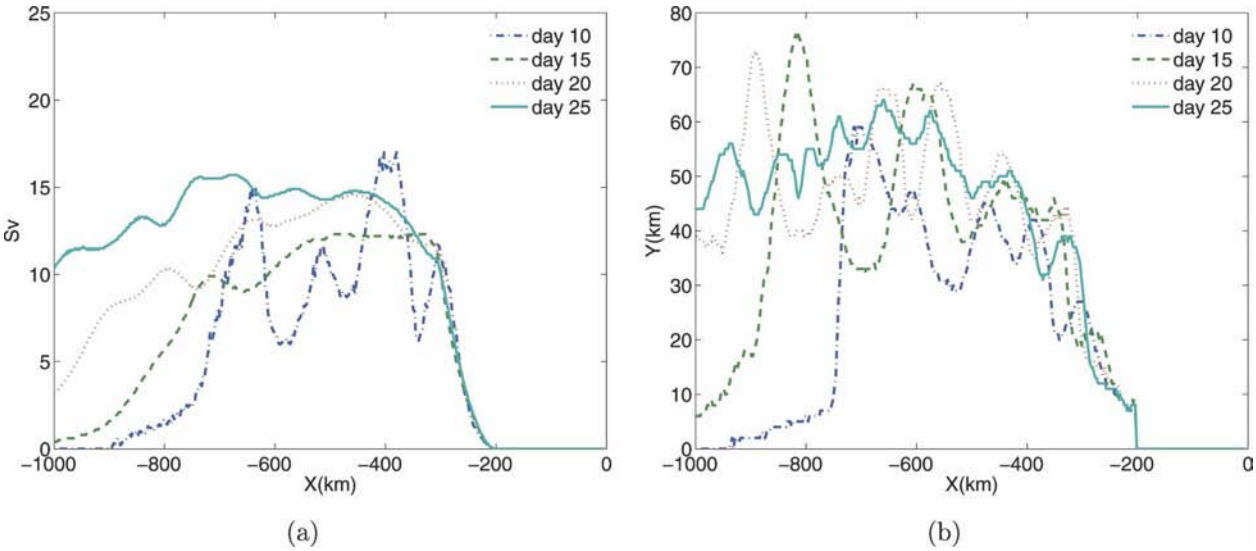

FIG. 6. (a) The longitudinal transport and (b) mean plume path in the case R3L on four different days.

ing the Coriolis force, the spectrum gap is reduced and shifted to lower frequency. The energy spectrum associated with the higher frequencies does not change much. However, when the Coriolis coefficient is increased by a factor of 2, the spectrum gap not only moves to higher frequency but also interacts with the small-scale feature.

Figures 5c and 5d illustrate the effects of horizontal and vertical background viscosity, respectively. The energy spectrum is very similar at low frequency. However, less energy is observed in the high frequency (small scale) with increasing either horizontal or vertical background viscosity. These results are consistent with the influence of different subgrid-scale models (i.e., different levels of turbulent viscosity) in common turbulent flow simulations (e.g., Tseng et al. 2006). It is clear that using very high horizontal viscosity largely overestimates the kinetic energy dissipation. When the explicit viscosity is small enough, the energy spectrum also converges well.

d. Entrainment and transport

By defining all fluid with tracer concentration $c > 1\%$ (Ω), we can calculate the total transport in the longitudinal direction as (Legg et al. 2006)

$$T(x) = \int_{\Omega} u(x, y, z)\, dy\, dz, \ \Omega \text{ is such that } c > 1\%, \quad (2)$$

where $u(x, y, z)$ is the longitudinal velocity. The spatial variation of transport is useful to diagnostic entrainment. Larger variation of transport associates with larger entrainment, which can efficiently enhance the momentum exchange and eddy intrusion. Figure 6 shows the instantaneous longitudinal transport and tracer mean plume path as a function of longitudinal distance on four different days. The mean path is defined by (Legg et al. 2006)

$$Y(x) = \frac{\int yC(x, y, z)\, dy\, dz}{\int C(x, y, z)\, dy\, dz}. \quad (3)$$

The time evolution shows quasi steady state is reached after 25 days for locations to the east of $x = -800$ km, although with some fluctuations associated with intensive eddy activity. To the west of $x = -800$ km, the flow is still evolving as the overflow water moves out of the domain. The transport increases from the imposed 5 Sv to about 12 Sv at $x = -300$ km, indicating strong diapycnal mixing and thus larger entrainment that increases the plume's volume. Farther downstream the mean plume path generally fluctuates. The oscillatory variation with a wavelength of roughly 100 km indicates some entrainment associated with meanders and eddies. The average plume thickness (proportional to the mean overflow path) increases rapidly initially ($x = -200$ to -400 km) and then gradually decreases and oscillates until the mean path approaches about 50–60 km offshore.

The time-averaged (15 days from model day 35 to day 50) longitudinal (along-slope) transport of the

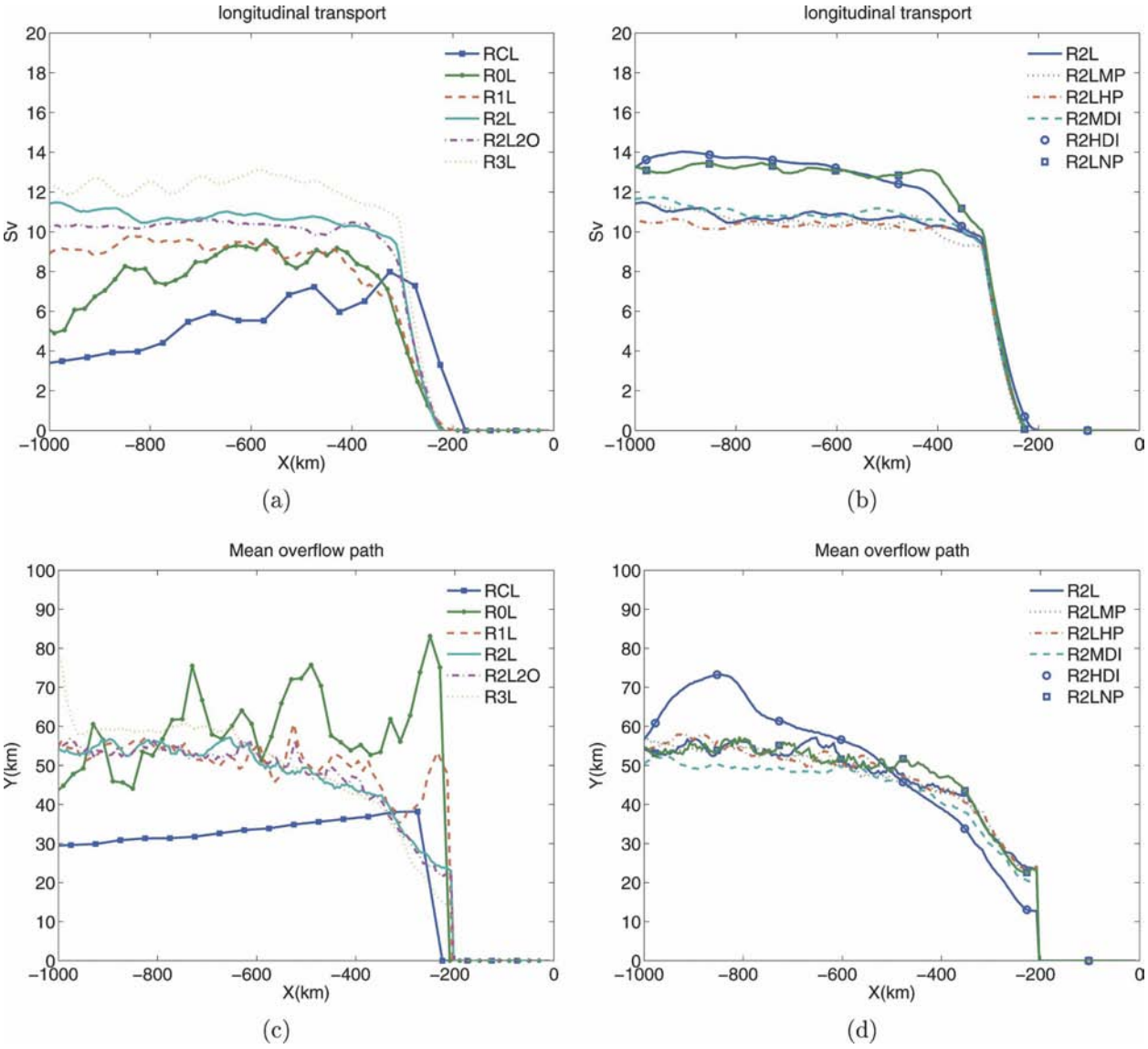

FIG. 7. Comparison of the longitudinal transport among different (a) resolutions and (b) viscosities from day 35 to day 50 for different runs. (c), (d) As in (a), (b) but for the mean plume path.

plume is compared in Figs. 7a and 7b for all runs. Less transport occurs in coarse-resolution runs (RCL, R0L, and R1L). This is associated with fewer eddies and slower longitudinal propagation in coarse-resolution cases. The decrease of entrainment for coarse-resolution runs has also been found in Legg et al. (2006). The time-averaged transport shows relatively constant transport and entrainment regardless of viscosity except for the runs with very high horizontal viscosity (R2HDI) and no vertical mixing parameterization (R2LNP). In general, significant entrainment (steep slope in the transport) mainly occurs in the area between $x = -200$ and -400 km. It is interesting to note that increasing horizontal viscosity and reducing vertical mixing parameterization have similar effects on the longitudinal transport. Larger transport in the R2HDI run probably associates with the bulk plume size, which also changes the mean overflow path (Fig. 7d); larger transport in the R2LNP run results from more energetic eddies, which thicken the plume vertically and do not change the mean plume path.

Figures 7c and 7d compare the same time-averaged (days 35–50) tracer plume mean path for all runs. The comparison shows that the time-averaged downstream mean paths align well with the longitudinal direction and are independent of resolution and viscosity except

for very coarse resolution runs. Slight increase (around 20%) is observed farther downstream ($x = -800$ km) in the high horizontal viscosity run (R2HDI). This is mainly due to the slower longitudinal penetration of bulk plume and simple diffusion effects evident in Fig. 4. The slightly broader mean plume path in the high horizontal viscosity run (R2HDI) suggests the possible increase in the downslope penetration as those shown in SPOM (Ezer and Mellor 2004). The introduction of eddies (from coarse to higher resolution) makes little difference to the mean overflow path downstream when the flow can be partially or fully resolved. However, the initial descent depends on the resolution greatly. For z-coordinate models, the most descent is seen in the R0L run, which is consistent with previous studies (Legg et al. 2006) and is because the plumes are not well resolved. Apparently, the plume mean path is not converging well within the range of common climate modeling resolution ($\Delta x = 50$ km for RCL run).

In the current study, the vertical mixing is estimated from Richardson number parameterization. Figures 8 and 9 compare the local gradient Richardson number Ri and vertical eddy diffusivity (κ_ν) for all runs. Larger eddy diffusivity implies the occurrence of significant vertical mixing. The local gradient Richardson number measures the local ratio between buoyancy and inertia:

$$\mathrm{Ri} = N^2/S^2, \tag{4}$$

where N is the Brunt–Väisälä frequency and $S^2 = (du/dz)^2 + (dv/dz)^2$. The snapshots are taken from a vertical–latitudinal section at 50 km downstream of the inflow on model day 60. Local Richardson number Ri is small near the bottom and coast. Figure 8 shows that low Ri is found over the whole dense overflow until it reaches neutral buoyancy, when Ri rapidly increases. The diapycnal mixing occur when low Ri occurs. The region of diapycnal mixing from 20 to 50 km offshore coincides with the region of low Ri, as required by the parameterization used. It is clear that the grid in RCL run is too coarse to resolve the region where diapycnal mixing occur.

The local gradient Richardson number Ri is used in the vertical mixing parameterization (Pacanowski and Philander 1981). The resulting eddy diffusivity κ_ν for the vertical mixing at the same time and location is illustrated in Fig. 8. A larger portion of high eddy diffusivity κ_ν is shown in coarse-resolution runs, which indicates larger vertical mixing. The increase of mixing in lower resolution is possibly because less extrema in shear are resolved. This shear may be the dominant cause of both mixing and entrainment due to baroclinic instability. Our result is consistent with the previous isopycnic model (Legg et al. 2006) where the entrainment is due to the vertically parameterized mixing. With reduced numerical mixing (sixth-order numerical diffusion) and vertical mixing parameterization, the converging property is as expected in the current study. Even in the run with second-order advection (R2L2O), the Ri and κ_ν distribution is quite similar to those in R2L. We believe our results can provide valuable guidance in refining the parameterizations and required resolution for the DOME configuration.

In addition, the structure of the plume near the bottom reveals an asymmetric spatial distribution of the eddy diffusivity with a large value close to the coast and a smaller value away from the coast. Higher eddy diffusivity implies significant mixing extending upward for over 200 m from the bottom while the smaller value indicates mixing is limited. Similar asymmetry has been found in previous simulations and observations on dense plumes over sloping bottoms (Ezer 2005; Girton and Sanford 2003). This is possible due to the Ekman bottom boundary dynamic, which causes the velocity to spiral from almost along isobath in the upper plume toward more downslope direction near the bottom (Ezer 2005). Again, small-scale noise is found in Fig. 8f and is consistent with the high-order, nondissipative numerical property. Increasing viscosity or using high-order, upwind-biased–monotonic numerical schemes will easily remove the noise. However, as noted above, we do not recommend using upwind-biased–monotonic schemes for turbulent mixing because the artificial dissipation/mixing is hard to quantify and depends on grid resolution (Ferziger and Tseng 2004).

Figure 9 shows the sensitivity of viscosity for medium resolution on the local gradient Richardson number and eddy diffusivity. In the large horizontal viscosity run (R2HDI), the eddies are strongly suppressed and low Ri region (with higher eddy viscosity) concentrates close to the bottom boundary near the coast. Using small background viscosity allows small-scale eddies to reduce the stratification and increase the kinetic energy in the nearshore region. The smaller Ri leads to increased vertical entertainment and mixing. These results are consistent with the viscous suppression of the shears that drive the parameterized mixing; thus the final plume density is higher. The vertical structure also depends greatly on the vertical mixing parameterization. Significant eddy activity and a large portion of low Ri region are observed in the case without vertical mixing parameterization (R2LNP run). Vertical mixing is difficult and only relies on background viscosity in this case. On the other hand, using extremely large vertical background viscosity (R2LHP run) interacts with the vertical parameterization scheme. Eddy viscosity is large in the whole field.

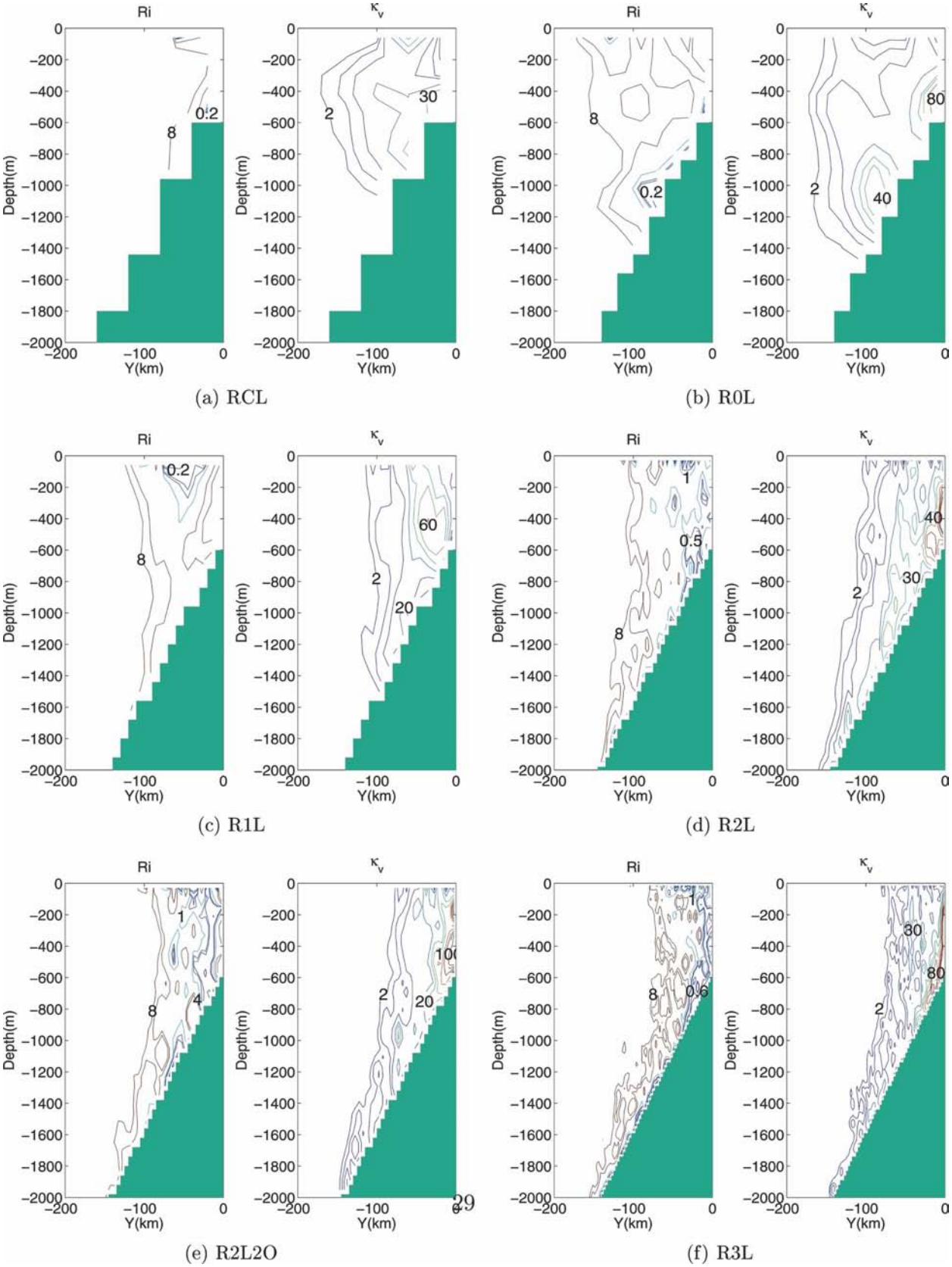

FIG. 8. Contours of Richardson number (Ri) and eddy diffusivity, κ_v (10^{-4} m^2 s^{-1}), along the 50-km downstream vertical–latitudinal section on day 60: Runs (a) RCL, (b) R0L, (c) R1L, (d) R2L, (e) R2L2O, and (f) R3L.

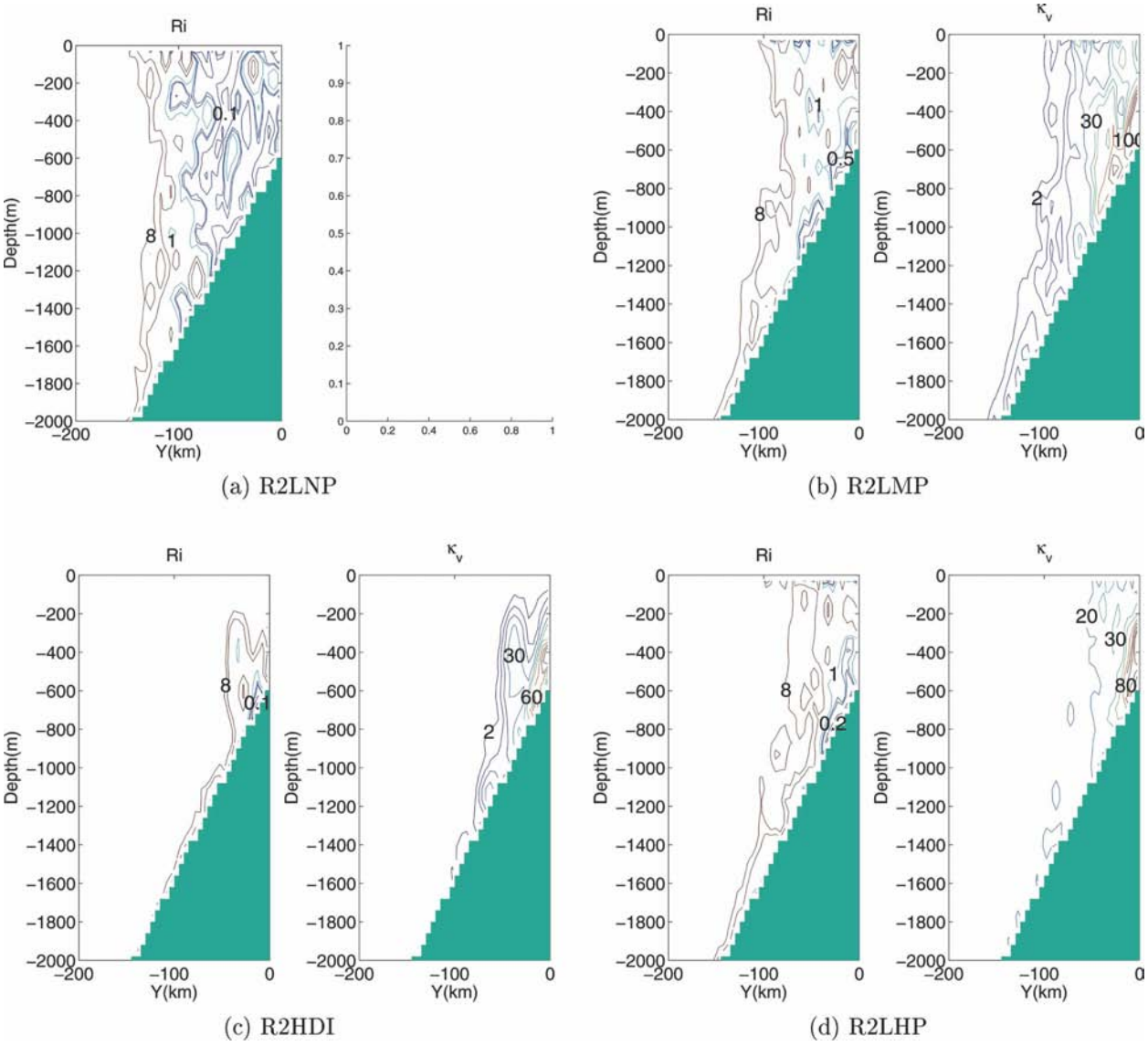

FIG. 9. As in Fig. 8 but for runs (a) R2LNP, (b) R2LMP, (c) R2HD1, and (d) R2LHP. Note that κ_v is zero for run (a) R2LNP because the vertical mixing scheme is turned off.

It is clear that the entrainment and mixing rely more on viscosity rather than resolution unless the resolution is extremely coarse. The effects of horizontal and vertical background viscosities are shown clearly. The medium-resolution runs with small background viscosity converge well to the highest-resolution run (R3LDI) in terms of eddy activity. The entrainment and mixing are found in the same location, which is consistent with the low Richardson number area.

e. Plume thickness and dilution

Figures 10 and 11 compare the tracer concentration in a vertical–latitudinal slice at the inflow and 50 km downstream from the inflow on model days 30 (Fig. 10a) and 60. The averaged plume thickness is roughly six to eight vertical grid intervals (150–200 m) in the R3L run (Fig. 10f) and is quite close to the observed plume downstream of the Denmark Strait (Girton and Sanford 2003). The plume thickness in coarse-resolution runs (Figs. 10a–d) is thicker since the density plume is only partially or not resolved. In the very coarse resolution run (Figs. 10a and 10b), it is evident that the flow cannot be resolved and the plume descends slowly, which is mainly dominated by diffusion (Legg et al. 2006; Ezer and Mellor 2004).

The grid convergence is clear from the simulations. Note that the realistic turbulent bottom boundary layer is not fully resolved by our calculations due to the

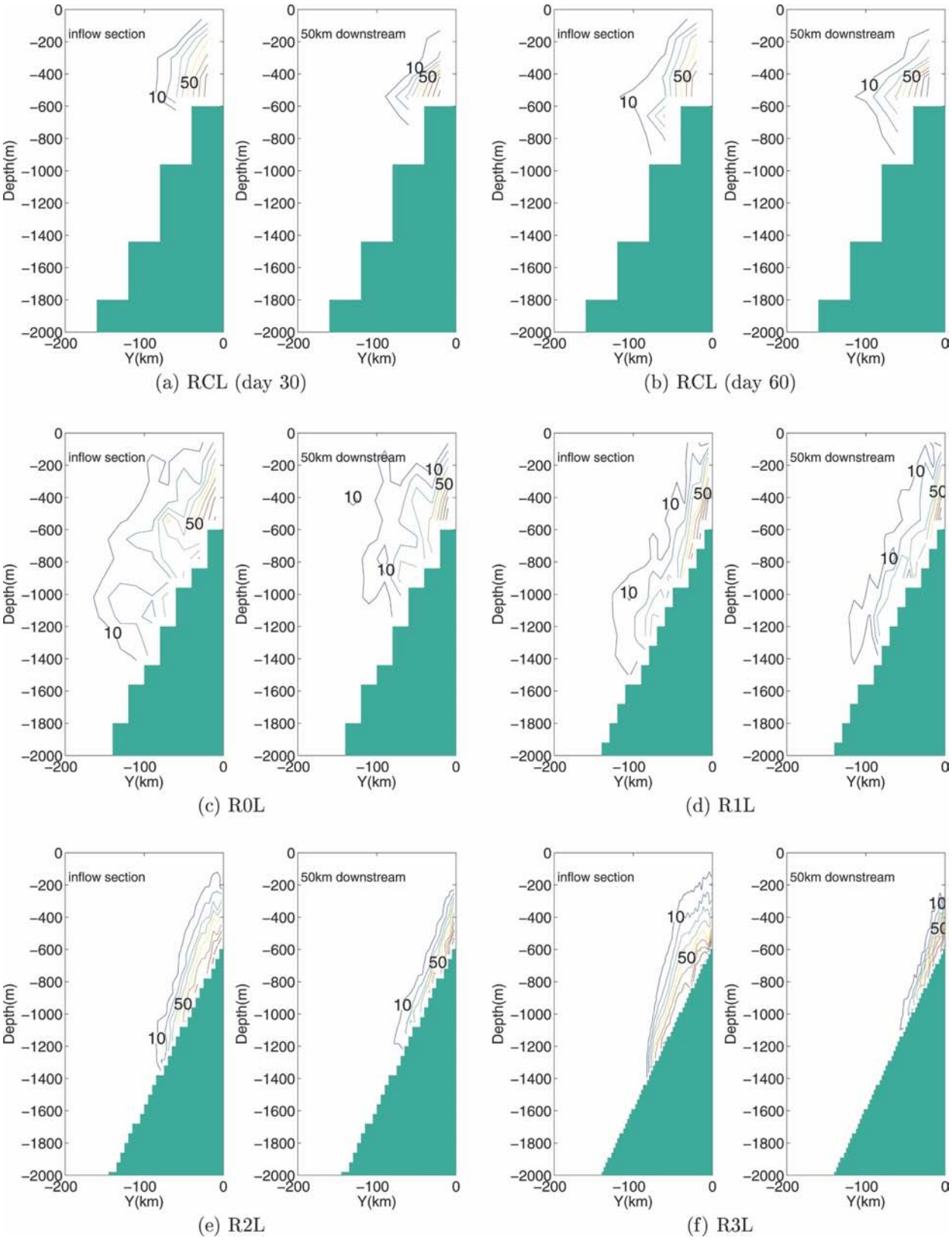

FIG. 10. Tracer concentration at the inflow vertical section and 50 km downstream on (a) model day 30 and (b)–(f) model day 60. The concentration is identified by percentage (%). Contours are plotted every 10%: Runs (a) RCL, (b) RCL, (c) R0L, (d) R1L, (e) R2L, and (f) R3L. The missing κ_v is intended because κ_v is zero within the whole domain.

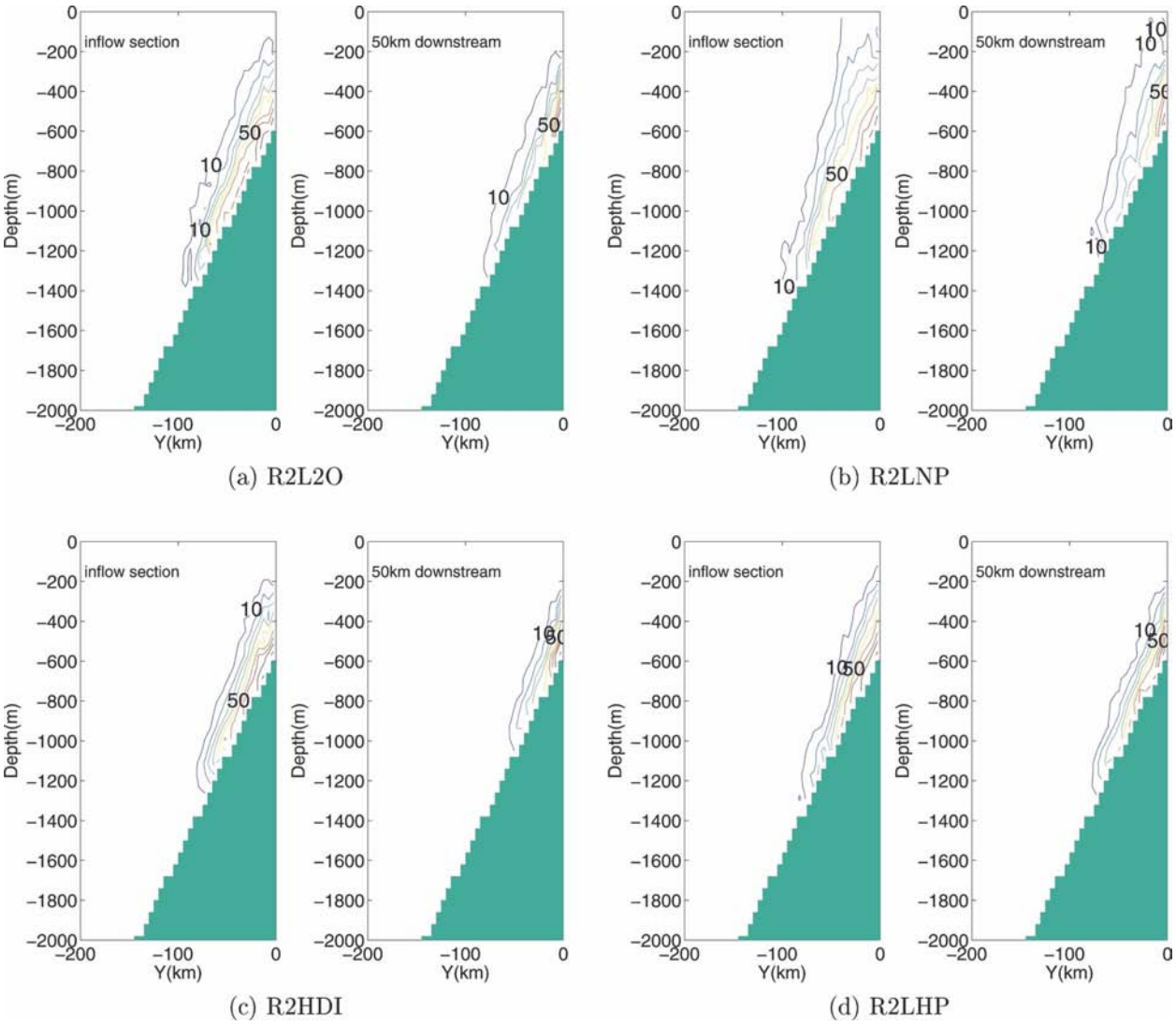

FIG. 11. Tracer concentration at the inflow vertical section and 50 km downstream on model day 60. The concentration is identified by percentage (%). Contours are plotted every 10%: Runs (a) R2L2O, (b) R2LNP, (c) R2HD1, and (d) R2LHP.

coarse vertical resolution and is beyond the scope of this study. The results in higher resolution show tighter fronts and more intense eddies, but otherwise show similar behaviors to the medium-resolution case shown.

In the medium 5-km resolution results (Fig. 11), the plume distribution along the slope is quite similar to the case with higher resolution. Slightly larger oscillation is observed in the R2L2O run because the dominant numerical error is third-order dispersion. The density plume appears thicker in the run without the vertical parameterization scheme (R2LNP). The thickening of the plume is mainly due to reduced stratification effects and more eddy entrainment due to larger vertical convection rather than vertical mixing. The effect of horizontal viscosity is quite small in terms of vertical structure. The downslope penetration seems not sensitive to the chosen diffusivity and the results are consistent with the mean overflow paths in Fig. 7.

Figures 12 and 13 show the tracer concentration along the vertical–longitudinal section at the northern boundary on model days 10 and 20. More energetic eddies and thicker plumes are observed in the low horizontal viscosity (R2L) and no vertical mixing parameterization (R2LNP) runs. These small-scale, frontal eddies can transport eddy energy upward more rapidly than the larger ones, thus reducing the stratification and increasing the kinetic energy in the upper layer, nearshore regions. These results are consistent with lower Ri region (Fig. 9) and clearly illustrate the influence of explicit viscosity in particular directions.

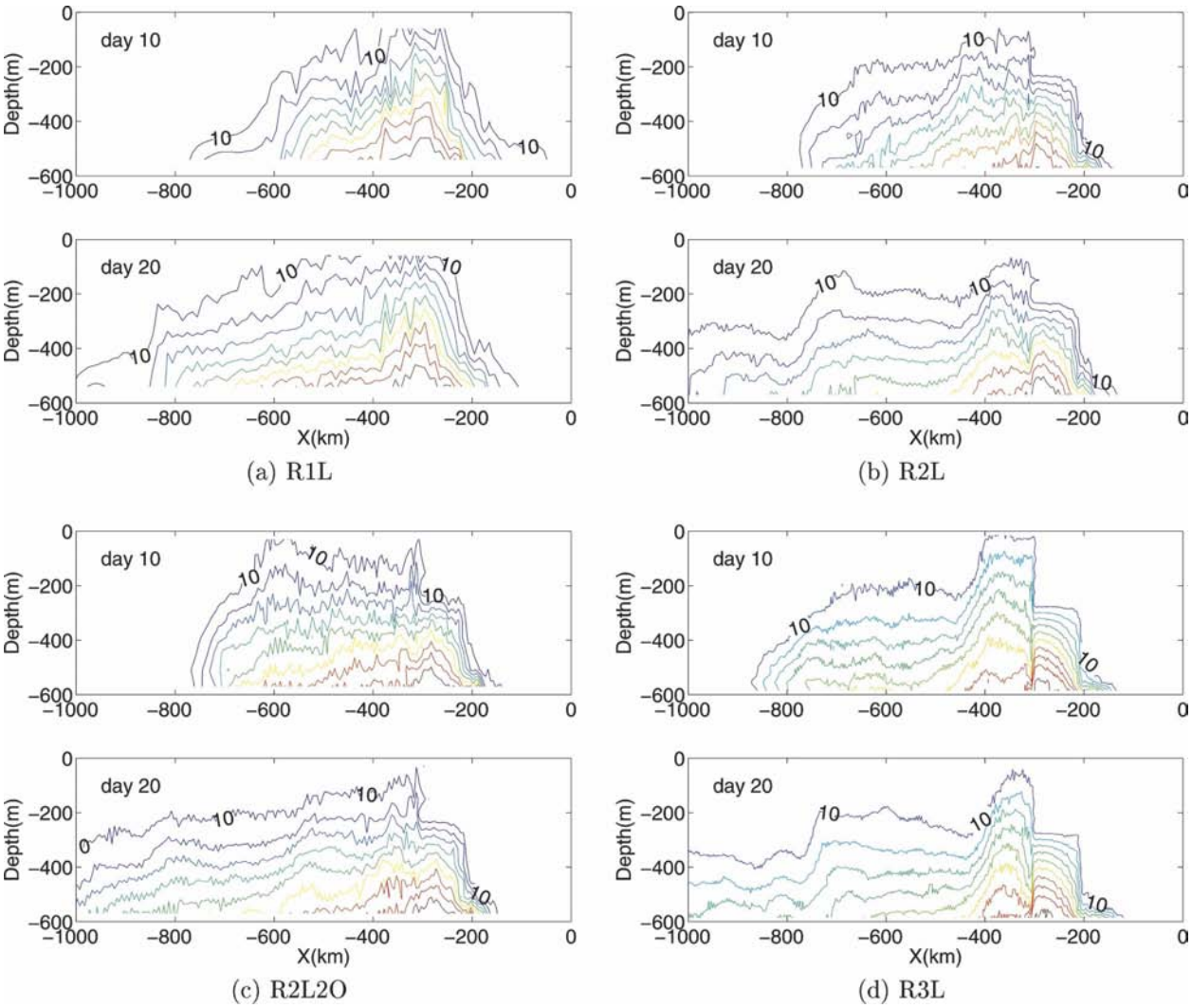

FIG. 12. Tracer concentration along the vertical–longitudinal section at the northern boundary on model days 10 and 20. The concentration is identified by percentage (%). Contours are plotted every 10%: Runs (a) R1L, (b) R2L, (c) R2L2O, and (d) R3L.

4. Discussion

a. Physical and numerical requirements for density current modeling

To get realistic downslope penetration, not only must one resolve the density current, but also one must not dilute it excessively when it flows downslope to its equilibrium level (where the ambient water matches its density). The density current equilibrium depth is affected by how much entrainment of the lower density ambient water occurs into the density current. Very little entrainment occurs in nature. This is further verified in a recent basin-scale, six-grid, two-way coupled North Atlantic Ocean and Mediterranean Sea simulation, where Mediterranean Sea Overflow Water (MOW) is successfully modeled with realistic penetration (~1000 m depth) and exchange (Dietrich et al. 2006, manuscript submitted to *J. Geophys. Res.*).

Excessive water-mass dilution in density currents by some early z-coordinate models seems exacerbated by invoking instant convective adjustment combining with the stair-step approximation of the bottom slope; that does not allow vertical advection to dominate as a density current flows toward deeper water over the edge of a stair step, and thus gives excessively dilutive physics that has no counterpart in nature. Excessive vertical and horizontal diffusivity near the bottom causes the same problem. This problem is not inherent to the z coordinate, but rather due to the assuming instant convective adjustment and/or excessive total (explicit and numerical) diffusion, which violates the weakly dilutive nature of density currents.

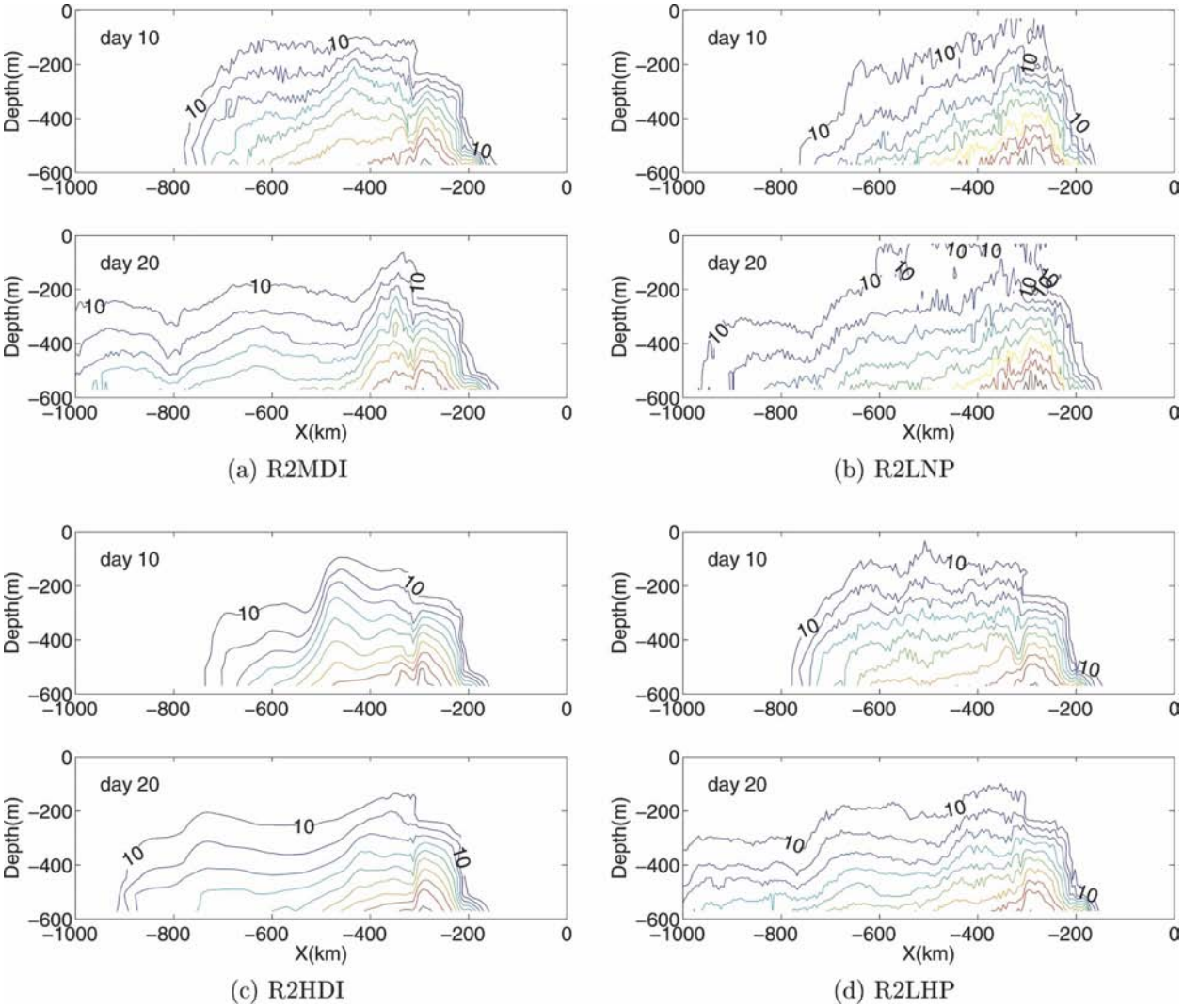

FIG. 13. As in Fig. 12 but for runs (a) R2MD1, (b) R2LNP, (c) R2HD1, and (d) R2LHP.

On the other hand, z-coordinate models that use a "C" grid may give deeper penetration than corresponding models using the "A" grid, because the Coriolis terms on the "C" grid vanish on a two-grid interval scale due to the numerical interpolations used in their evaluation. They are also too small on larger, but barely resolved scales. When combined with low dissipation, this allows vortex stretching on the smallest resolved scale by reducing the vortex stretching constraint from the Coriolis terms. The weaker penetration in the coarsest grid result (RCL) may partially relate to the strong vortex stretching constraint that exists on the smallest resolved scale.

Our results are also consistent with earlier studies showing that the density current water does not penetrate far enough downslope when the resolution is extremely coarse (Legg et al. 2006; Winton et al. 1998), especially due to strong rotational constraints on the resolved scales. However, even in the coarsest grid (RCL) herein, the plume is clearly hugging the bottom and penetrating to deeper water by a slower downslope flow component (Figs. 8 and 10). The Coriolis terms may somewhat overconstrain downslope penetration when the resolution is too coarse, but this is a resolution limitation that is not unique to z-coordinate models.

b. *Adequacy of z-coordinate models for DOME setup*

Our grid resolution study shows that the main features of the DOME density current converge to the correct, low-dilution solution as its resolution increases. This is as expected in terms of its physics and numerics. These results clearly show that the current z-coordinate

model is appropriate for the DOME configuration without the need for excessive background viscosity/diffusivity and allows clear sensitivity analysis. It is found that z-coordinate models can accurately model density currents, including downslope deep penetration, if the resolution is fine enough to resolve the density current (i.e., the plume thickness is at least triple of the grid resolution, 5 km in the current DOME setup). At intermediate resolution, our purely z-coordinate model results adequately describe many density current features if viscosity/diffusion (both explicit and numerical) is small and highly dilutive instant convective adjustment is not invoked.

We choose not to optimize the z-coordinate representation in this study in order to relate the overall performance to the general variable slope problem. Note that such a constant slope is ideal for σ-coordinate models because a uniform slope avoids density gradient noise from complicated bathymetry. High-order and conservative numerics avoid numerical instability. The other alternative is to use high viscosity/diffusivity to stabilize the simulation suggested by previous studies (Ezer and Mellor 2004), but is not recommended here.

The poor behavior of previous purely z-coordinate model (e.g., Beckmann and Doscher 1997; Ezer and Mellor 2004) may result from the large viscosity and diffusivity as demonstrated in our higher-viscosity comparison. This is because, as D04 showed, using larger viscosity (50 $m^2 s^{-1}$) strongly damps the density currents. Such currents under the Gulf Stream are greatly weakened by the time they reach the Cape Cod region from their sources, which are a few thousand kilometers upstream in the Greenland–Iceland–Norway (GIN) Sea. With excessive numerical dissipation they are too weak to continue into the New York Bight against an energetic Gulf Stream current and thereby unrealistically affect Gulf Stream separation and path. Ezer and Mellor (1992) show such sensitivity in a focused regional study in which the density current is a specified inflow, as do Thompson and Schmitz (1989).

Even though the z-coordinate is adequate for idealized DOME setup, it is noteworthy that downslope density current penetration may be mainly controlled by bottom boundary layer secondary (downslope) flows due to the actual dissipation that occurs in nature (Ezer 1990). Without such dissipation, the Coriolis terms arrest downslope flow of density currents. Once baroclinic instability effects are in quasi-equilibrium with the currents, the eddies dissipate downstream from sill overflows. Our results suggest that such quasi-equilibrium may already exist upstream of the real sill overflows in nature, because stronger eddies are observed near the open-sill overflow boundary (geostrophically balanced) in the simulation. Thus, bottom boundary layer resolution and numerics may significantly affect downslope density current penetration, and it may be useful to include a thin-shell bottom boundary layer approach (e.g., Dietrich et al. 1987; Song and Chao 2000), but that is a separate issue from the discussion of z-coordinate models outside the bottom boundary layer.

5. Concluding remarks

A purely z-coordinate DieCAST model without special topography treatment was shown to give robust bottom density currents in an idealized overflow configuration patterned after the flow in the Denmark Strait region. Although there is no observation for the idealized DOME configuration, the convergence of the grid resolution study illustrated the required resolution to resolve the flow using a purely z-coordinate model. It is found that 5- or 2.5-km resolution can fully resolve the overflow plumes that have thickness of roughly 150–200 m in the idealized DOME configuration (necessary condition). The downslope plume hugs the bottom all the way to the western outflow. The downslope penetration and thickness are similar to the observed results, as reported by Ezer and Mellor (2004). The density current frequently pinches off eddies that propagate westward along the idealized shelf slope.

The numerical results are independent of resolution when the grid is fine enough to resolve the large-scale features (e.g., the plume thickness and Rossby radius). More finer-scale features with reduced magnitude of oscillation are observed using the fourth-order nondissipative advection scheme rather than the second-order one. The effects of background viscosity/diffusivity play more important roles on the entrainment and transport of density current. These are quantified through a series of sensitivity studies. Effects of increasing horizontal viscosity include reduced penetration, reduced small-scale eddies, stronger stratification, and slower propagation of the plume. The results show good convergence of the resolved flow with increasing resolution or decreasing viscosity.

The severe robustness and accuracy problems of the ZPOM results reported in Ezer and Mellor (2004) were never seen in the current z-coordinate model. The poor ZPOM results may be due to the numerics rather than the chosen coordinate itself as shown in our comparison. The bottom density currents were also modeled in the application of full real North Atlantic basin (D04) without a BBL model. The behavior of thin, narrow bottom density currents is very sensitive to model viscosity and diffusivity (D04) if the background viscosity

is not small enough, which could be one reason for the corresponding poor ZPOM results.

In fact, the thin-shell BBL approach (Dietrich et al. 1987; Song and Chao 2000) combined with IBM (Tseng and Ferziger 2003; Tseng et al. 2005) would have a big advantage over the purely σ-coordinate approach due to its elimination of problems associated with baroclinic pressure gradient evaluation (Haney 1991) or confining them to the BBL. In view of the strongly dissipative physics of the turbulent BBL underlying the density currents, a successful BBL model must include a good subgrid-scale turbulence closure, as did the SOMS model in studying an idealized density current (Ezer 1990). On the other hand, the requirements for modeling the low dissipation overlying density current are different: robustness and accuracy of the resolved flow scales are more important than representation of subgrid-scale effects on the resolved flow.

Acknowledgments. We warmly thank Bob Haney for encouraging and previewing this note. We also thank Avichal Mehra, Harley Hurlburt, Aaron Lai, Paul Martin, Steve Piacsek, Jim Richman, and Dan Wright for their encouragement to write a note clearly showing a z-coordinate model can simulate bottom density current well with low viscosity. We really want to thank Tal Ezer for his valuable comments, suggestions, and clarification, and Helen He for the discussion of MPH library. Finally, the insightful comments and suggestions from Matthew Hecht and the other, anonymous reviewer are greatly appreciated. The first author is supported by DOE SciDAC Climate Project and funding from the Department of Atmospheric Sciences, National Taiwan University.

REFERENCES

Adcroft, A., C. Hill, and J. Marshall, 1997: Representation of topography by shaved cells in a height coordinate ocean model. *Mon. Wea. Rev.,* **125,** 2293–2315.

Beckmann, A., and R. Doscher, 1997: A method for improved representation of dense water spreading over topography in geopotential-coordinate models. *J. Phys. Oceanogr.,* **27,** 581–591.

Cenedese, C., J. A. Whitehead, T. Ascarelli, and M. Ohiwa, 2004: A dense current flowing down a sloping bottom in a rotating fluid. *J. Phys. Oceanogr.,* **34,** 188–203.

Dietrich, D. E., 1977: Direct simulation of convective adjustment and other ensemble effects. *Atmosphere,* **15,** 1–18.

——, 1997: Application of a modified "a" grid ocean model having reduced numerical dispersion to the Gulf of Mexico circulation. *Dyn. Atmos. Oceans,* **27,** 201–217.

——, M. G. Marietta, and P. J. Roache, 1987: An ocean modeling system with turbulent boundary layers and topography: Part 1. Numerical studies of small island wakes in the ocean. *Int. J. Numer. Methods Fluids,* **7,** 833–855.

——, A. Mehra, R. L. Haney, M. J. Bowman, and Y. H. Tseng, 2004: Dissipation effects in modeling the North Atlantic Ocean. *Geophys. Res. Lett.,* **31,** L05302, doi:10.1029/2003GL019015.

Ezer, T., 1990: A numerical study of the interaction between a deep cold jet and the bottom boundary layer of the ocean. *J. Phys. Oceanogr.,* **20,** 801–816.

——, 2005: Entrainment, diapycnal mixing and transport in three-dimensional bottom gravity current simulations using the Mellor–Yamada turbulence scheme. *Ocean Modell.,* **9,** 151–168.

——, and G. L. Mellor, 1992: A numerical study of the variability and the separation of the Gulf Stream, induced by surface atmospheric forcing and lateral boundary flows. *J. Phys. Oceanogr.,* **22,** 660–682.

——, and ——, 2004: A generalized coordinate ocean model and a comparison of the bottom boundary layer dynamics in terrain-following and in z-level grid. *Ocean Modell.,* **6,** 379–403.

Ferziger, J. H., and M. Perić, 2002: *Computational Methods for Fluid Dynamics.* 3d ed. Springer-Verlag, 423 pp.

——, and Y. H. Tseng, 2004: A coordinate system independent streamwise upwind method for fluid flow computation. *Int. J. Numer. Methods Fluids,* **45,** 1235–1247.

Girton, J. B., and T. B. Sanford, 2003: Descent and modification of the overflow plume in the Denmark Strait. *J. Phys. Oceanogr.,* **33,** 1351–1364.

Gresho, P. M., and R. L. Lee, 1981: Don't suppress the wiggles—They're telling you something. *Comput. Fluids,* **9,** 223–253.

Haney, R. L., 1991: On the pressure gradient force over steep topography in sigma coordinate ocean models. *J. Phys. Oceanogr.,* **21,** 610–619.

He, Y., and C. H. Q. Ding, 2005: Coupling multi-component models with MPH on distributed memory computer architectures. *Int. J. High Perform. Comput. Appl.,* **19,** 329–340.

Jiang, L., and R. W. Garwood, 1996: Three-dimensional simulations of overflows on continental slopes. *J. Phys. Oceanogr.,* **26,** 1214–1233.

Killworth, P. D., 2001: On the rate of descent of overflows. *J. Geophys. Res.,* **106,** 22 267–22 275.

——, and N. R. Edwards, 1999: A turbulent bottom boundary layer code for use in numerical ocean models. *J. Phys. Oceanogr.,* **29,** 1221–1238.

Kravchenko, A. G., and P. Moin, 2000: Numerical studies of flow over a circular cylinder at $Re_D = 3900$. *Phys. Fluids,* **12,** 403–417.

Legg, S., R. W. Hallberg, and J. B. Girton, 2006: Comparison of entrainment in overflows simulated by z-coordinate, isopycnal and nonhydrostatic models. *Ocean Modell.,* **11,** 69–97.

Lilly, D. K., 1965: On the computational stability of numerical solutions of time-dependent non-linear geophysical fluid dynamics problems. *Mon. Wea. Rev.,* **93,** 11–26.

Mittal, R., and P. Moin, 1997: Suitability of upwind-biased finite difference schemes for large-eddy simulation of turbulent flows. *AIAA J.,* **35,** 1415–1417.

Pacanowski, R. C., and S. G. H. Philander, 1981: Parameterization of vertical mixing in numerical models of tropical ocean. *J. Phys. Oceanogr.,* **11,** 1443–1451.

——, and A. Gnanadesikan, 1998: Transient response in a z-level ocean model that resolves topography with partial cells. *Mon. Wea. Rev.,* **126,** 3248–3270.

Penduff, T., B. Barnier, M.-A. Kerbiriou, and J. Verron, 2002: How topographic smoothing contributes to differences between the eddy flows simulated by sigma- and geopotential-coordinate system. *J. Phys. Oceanogr.,* **32,** 122–137.

Peters, H., W. E. Johns, A. S. Bower, and D. M. Fratantoni, 2005: Mixing and entrainment in the Red Sea outflow plume. Part II: Plume structure. *J. Phys. Oceanogr.,* **35,** 569–583.

Pouquet, A., U. Frisch, and J. P. Chollet, 1983: Turbulence with a spectral gap. *Phys. Fluids,* **26,** 877–880.

Sanderson, B. G., 1998: Order and resolution for computational ocean dynamics. *J. Phys. Oceanogr.,* **28,** 1271–1286.

Song, Y. T., and Y. Chao, 2000: An embedded bottom boundary layer formulation for z-coordinate ocean models. *J. Atmos. Oceanic Technol.,* **17,** 546–560.

Thompson, J. D., and W. J. Schmitz, 1989: A limited-area model of the Gulf Stream: Design, initial experiments and model-data intercomparison. *J. Phys. Oceanogr.,* **19,** 791–814.

Tseng, Y. H., and J. H. Ferziger, 2001: Mixing and available potential energy in stratified flows. *Phys. Fluids,* **13,** 1281–1293.

——, and ——, 2003: A ghost-cell immersed boundary method for flow in complex geometry. *J. Comput. Phys.,* **192,** 593–623.

——, and ——, 2004: Large-eddy simulation of turbulent wavy boundary flow—Illustration of vortex dynamics. *J. Turbulence,* **5,** 034.

——, and D. E. Dietrich, 2005: Guide for the DieCAST Ocean Model. 44 pp. [Available online at http://oceanmodels.coas.oregonstate.edu/DieCOM/publications/users_manual.pdf.]

——, ——, and J. H. Ferziger, 2005: Regional circulation of the Monterey Bay region—Hydrostatic versus non-hydrostatic modeling. *J. Geophys. Res.,* **110,** C09015, doi:10.1029/2003JC002153.

——, C. Meneveau, and M. B. Parlange, 2006: Modelling flow around bluff bodies and urban dispersion using large eddy simulation. *Environ. Sci. Technol.,* **40,** 2653–2662.

Van der Hoven, I., 1957: Power spectrum of horizontal wind speed in the frequency range from 0.0007 to 900 cycles per hour. *J. Meteor.,* **14,** 160–164.

Winton, M., R. Hallberg, and A. Gnanadesikan, 1998: Simulation of density driven frictional downslope flow in *z*-coordinate ocean models. *J. Phys. Oceanogr.,* **28,** 2163–2174.